International Journal of Robotics and Control Systems
Vol. 5, No. 2, 2025, pp. 1139-1155
ISSN 2775-2658
http://pubs2.ascee.org/index.php/ijrcs

Collision Avoidance in Mini Autonomous Electric Vehicles Using Artificial Potential Fields for Outdoor Environment

Joko Slamet Saputro [a,1,*], Hanif Wisti Juliatama [a,2], Feri Adriyanto [a,3] Hari Maghfiroh [a,4]
Esa Apriaskar [b,c,5]

[a] Department of Electrical Engineering, Universitas Sebelas Maret, Jl. Ir Sutami 36 Kentingan Jebres, Surakarta, 57126, Indonesia
[b] Department of Electrical Engineering, Universitas Negeri Semarang, Gunungpati, Semarang, 50229, Indonesia
[c] School of Electrical and Electronic Engineering, University of Sheffield, Sheffield, S10 2TN, United Kingdom
[1] jssaputro89@staff.uns.ac.id; [2] hanifwistijulitama@student.uns.ac.id; [3] feri.adriyanto@staff.uns.ac.id;
[4] hari.maghfiroh@staff.uns.ac.id; [5] eapriaskar1@sheffield.ac.uk
* Corresponding Author

ARTICLE INFO

Article history
Received November 15, 2024
Revised April 23, 2025
Accepted April 30, 2025

Keywords
Autonomous Electric Vehicle;
Collision Avoidance;
Potential Field;
LiDAR;
ADAS

ABSTRACT

The rapid advancement of technology is driving the transition toward Society 5.0, where intelligent transportation systems enhance safety, efficiency, and sustainability. One of the biggest challenges in transportation is the high frequency of vehicle accidents, with approximately 80% attributed to driver error. To mitigate this, Advanced Driver Assistance Systems (ADAS) have been developed to improve vehicle autonomy and reduce accidents. This research proposes a potential field-based collision avoidance system for autonomous vehicle navigation, where the vehicle and obstacles act as positive poles, repelling each other, while the target destination serves as a negative pole, attracting the vehicle. Experimental results demonstrate a GPS positioning error of 1.55 m with a 66% success rate and LiDAR sensor accuracy of 96.4%, exceeding the required 95% threshold. Obstacle avoidance was tested with two safety thresholds (2 m and 2.5 m) across single- and two-obstacle scenarios. The 2 m threshold resulted in shorter travel distances (16.406 m vs. 16.535 m for 2.5 m) and faster completion times (19.036 s vs. 19.144 s), while the 2.5 m threshold provided greater clearance. GPS accuracy was significantly influenced by HDOP values and satellite count, with lower HDOP improving trajectory precision. The system successfully adjusted its trajectory in response to obstacles, ensuring effective real-time navigation.

1. Introduction

Traffic accidents remain a critical global concern, with data from the World Health Organization (WHO) indicating that approximately 1.25 million fatalities occur annually due to road accidents [1]. Each year, the United States records over 6.4 million vehicle accidents [2]. Studies suggest that over 80% of these accidents are attributed to driver errors, which stem from factors such as fatigue, lack of concentration, inadequate road lighting, mobile phone distractions, and complex terrain conditions [3]-[5] . While modern vehicles are equipped with passive safety features like airbags and seat belts to mitigate accident impact, these systems primarily function after a collision has already occurred

[6]. Therefore, to proactively reduce accident risks, the development of Advanced Driver Assistance Systems (ADAS) is essential [7]-[9].

ADAS is an integrated safety system that enhances vehicle automation by utilizing various sensors, such as cameras, LiDAR (Light Detection and Ranging), radar, and ultrasonic sensors, to detect the surrounding environment and support real-time decision-making [10]. Key ADAS features include adaptive cruise control (ACC) [11], road recognition, lane departure warning, inteligent speed assistant, collision prevention [12], and automatic emergancy braking [13]. Among these, collision prevention is particularly critical for autonomous vehicles, as it ensures safe navigation by identifying and avoiding obstacles. Traditionally, cameras have been widely used for object detection [14]-[18]; however, they are highly sensitive to lighting conditions, have limited range, and create blind spots due to their unidirectional coverage [19]. To address these limitations, LiDAR has emerged as a more robust alternative for collision detection [20]. Unlike cameras, LiDAR is unaffected by ambient lighting, as it operates by emitting infrared laser pulses and measuring their reflection time to determine object distances [21]. However, integrating LiDAR into an efficient collision avoidance system requires an effective path-planning algorithm [22]-[24].

ADAS represents a transformative technology that has significantly reshaped vehicle safety. The primary goal is to enhance driving safety by utilizing advanced technology capable of detecting obstacles, alerting drivers, and even taking automated action when necessary. ADAS has made considerable strides in advancing road safety and reducing accidents, marking a crucial step toward a future where fully autonomous vehicles can navigate without driver assistance. However, reaching full autonomy requires progressing through multiple levels of ADAS, which reflect the technology's current capabilities and the driver's role. The Society of Automotive Engineers (SAE) has established a widely recognized framework that categorizes ADAS into levels based on the degree of automation and the driver's role in controlling the vehicle, as shown in Fig. 1 [25], [26]. The first three SAE levels (0, 1, and 2) focus on driver assistance by providing warnings or interventions while requiring the driver to remain fully aware of their surroundings. In contrast, levels 3, 4, and 5 introduce increasing levels of automation, ranging from partial control shared between the system and the driver to full autonomy [27].

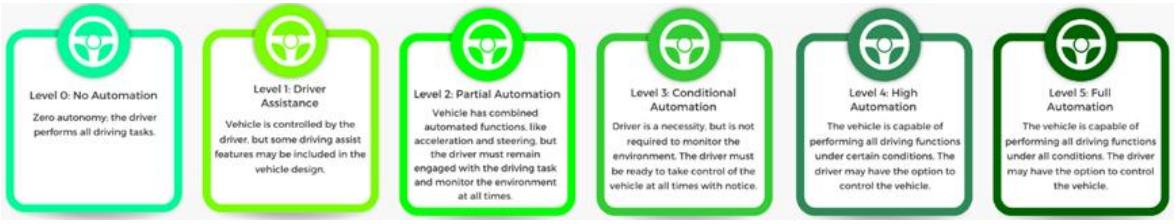

Fig. 1. Autonomous driving levels [26]

In recent research, an ADAS system was developed with two main features: collision prevention (Level 2) and automatic navigation using GPS (Level 3). Both systems work together to avoid surrounding objects and guide the vehicle to its destination through GPS-based navigation. The collision prevention feature operates using sensors such as LiDAR, radar, ultrasonic sensors, and strategically positioned cameras to monitor the environment. A notable advantage of this system is its ability to respond in various ways, including issuing warnings, providing information to the driver, applying emergency braking, and adjusting the vehicle's path to avoid collisions. Meanwhile, the automatic navigation system uses GPS technology to help the vehicle reach its destination without driver intervention. This means vehicles can follow pre-programmed routes and adapt to potential changes along the way. However, to improve collision avoidance effectiveness, real-time path-planning algorithms are needed to ensure the vehicle dynamically responds to changing environments.

An autonomous vehicle is a type of car capable of operating in unfamiliar or previously unexplored environments [28]. This vehicle can move toward a goal independently and can avoid surrounding obstacles. To achieve this level of autonomy, autonomous vehicles are equipped with

various sensors, such as an Inertial Measurement Unit (IMU), GPS, and LiDAR, which serve as the foundation for navigation. These sensors not only allow the vehicle to follow predetermined paths but also function as real-time object detectors, enabling immediate obstacle response and adaptive path adjustments [29].

In this research, a collision avoidance system was developed based on a two-dimensional, 360-degree LiDAR sensor. LiDAR was selected for its ability to thoroughly detect objects in all directions, including in areas not typically visible to a driver. Moreover, it is independent of weather conditions and has a longer detection range than acoustic and optical sensors [30]-[32]. The system utilizes the Potential Field Method (PFM), which is widely used in robotic navigation due to its ability to generate repulsive forces between objects, ensuring the vehicle follows a safe path [33]. The key advantage of PFM-based navigation is its ability to operate in dynamic environments, adjusting the vehicle's trajectory in real time to avoid potential collisions [34]-[36].

To validate the proposed system, a 1/12 scale Radio Control (RC) car was used to simulate an autonomous vehicle shown in Fig. 2. This car is equipped with an Ackermann steering system, a DC motor for propulsion, and a servo for controlling the front-wheel steering. The scaled model serves as a testbed for evaluating ADAS technologies, allowing for the practical development of autonomous navigation strategies. By combining LiDAR-based perception with the PFM algorithm, this research aims to enhance collision avoidance performance, contributing to the advancement of autonomous vehicle safety. Such developments mark an important step toward achieving fully autonomous navigation in real-world scenarios.

Fig. 2. RC-car scale 1/12

2. Material and Method

2.1. Hardware Design

The block diagram of the entire system is shown in Fig. 3. The primary sensor used in this project is the RPLIDAR A3M1 LiDAR, which enables 360-degree environmental scanning for object detection. This wide scanning range allows the system to generate an accurate real-time map of the surroundings. The Raspberry Pi 4 serves as the main processing unit, handling LiDAR data to measure distances and determine the sensor's orientation for precise object detection. For positioning and navigation, the system integrates Radiolink's SE100 GPS sensor, which provides real-time location data, ensuring the vehicle follows its designated path autonomously without human intervention.

The electronics system connection is illustrated in Fig. 4. The key electronic components include: Pixhawk 2.4.8 controller – serves as the vehicle's main control unit for autonomous operation; Steering servo – controls the vehicle's directional movement; Brushed DC motor –

provides propulsion; 360-degree LiDAR sensor – detects obstacles and maps the environment; Electronic Speed Controller (ESC) – regulates the speed of the DC motor [37]-[39]; Telemetry module – facilitates real-time data communication with a development laptop; and Receiver – enables wireless control signals.

The servo and DC motor receive PWM signals from Pixhawk 2.4.8, allowing for precise control over steering and speed adjustments [40]. A LiPo battery (7.4 V 5400 mAh) powers the vehicle. A step-down DC-DC converter that reduces DC voltage from the battery to ensure a stable 5V supply for the Pixhawk microcontroller [41]. Additionally, the ESC manages power delivery to the driving motor. Telemetry communication enables real-time data monitoring and control during vehicle testing, ensuring efficient debugging and performance evaluation.

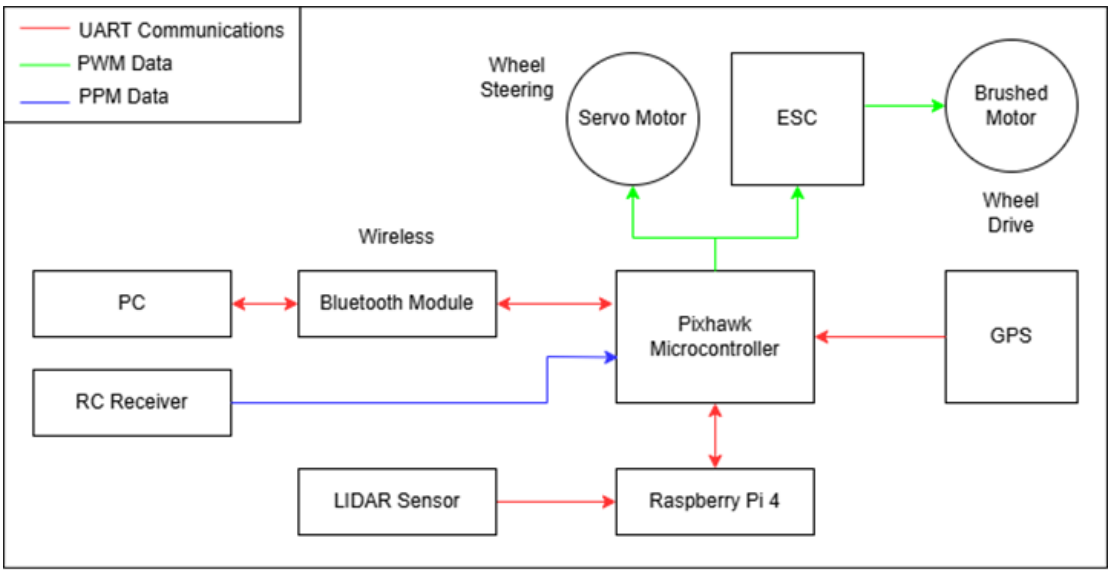

Fig. 3. Block diagrams of the whole system

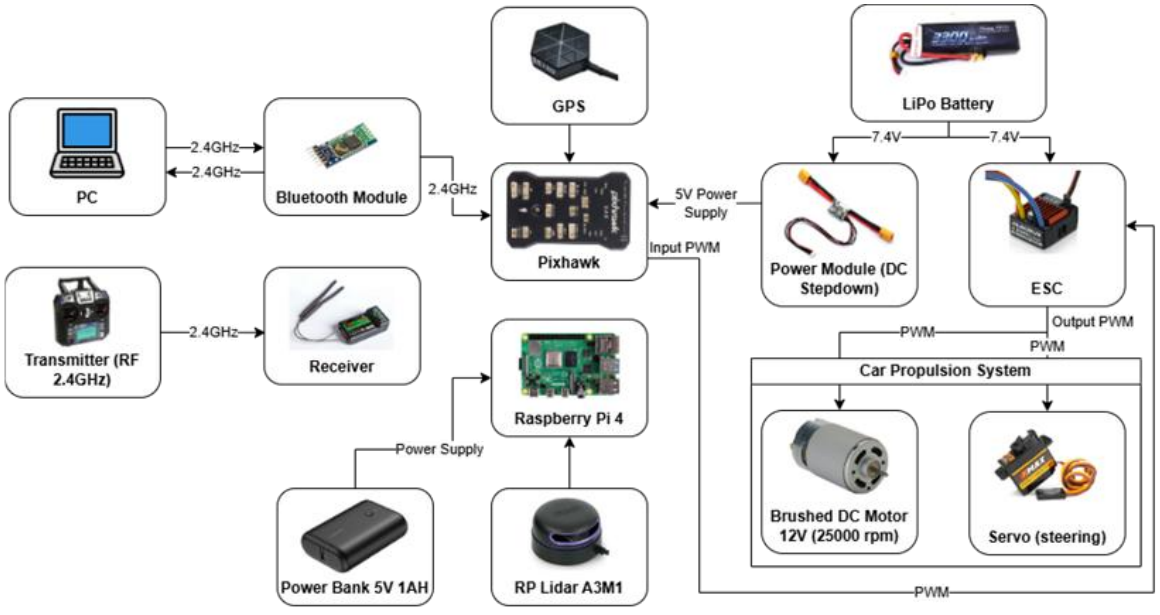

Fig. 4. Electronics system

2.2. System Design

This phase focuses on implementing the potential field method to develop an active collision avoidance system that autonomously steers the vehicle around obstacles while following the shortest,

obstacle-free route to its destination. A 360-degree LiDAR sensor is employed to detect objects at distances exceeding 5 meters, ensuring effective and responsive collision avoidance.

2.2.1. Potential Field Method for Lidar Sensor Data Processing

In this stage, the potential field method is utilized to create a crash-avoidance system, enabling the vehicle to autonomously navigate toward its target while avoiding obstacles, even if they appear directly in its path [42]. The system identifies the shortest safe route by leveraging 360-degree LiDAR data, which provides precise distance measurements between the vehicle and surrounding objects. Within the potential field framework, the vehicle is treated as a particle moving in a potential field, where the destination point acts as a negative charge that attracts the vehicle, while obstacles are represented as positive charges that generate repulsive forces [43]. These attractive and repulsive forces interact to guide the vehicle along a collision-free path [44], as illustrated in Fig. 5. The optimal route is determined through potential field calculations using equations (1)-(3), ensuring real-time decision-making for autonomous navigation.

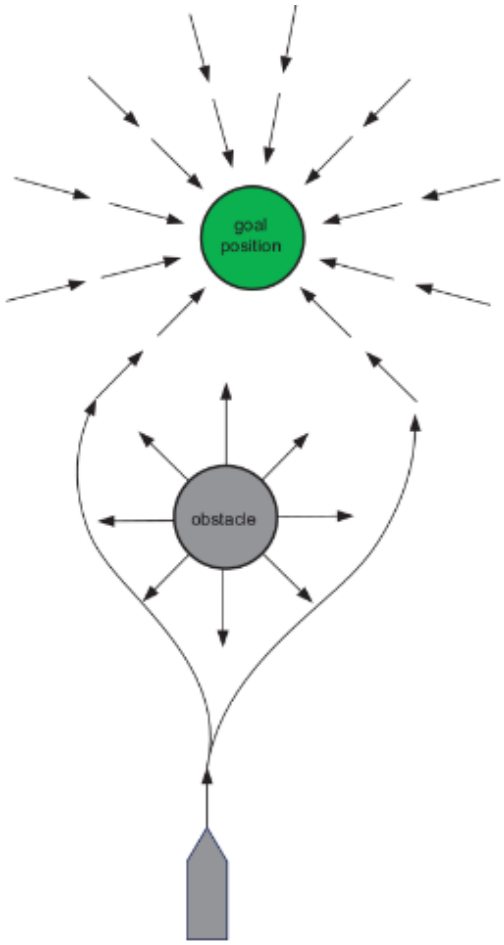

Fig. 5. Potential field method [44]

$$f_{total} = f_{Pull} + f_{repulsive} \tag{1}$$

$$f_{Pull} = k_{Pull} \frac{p_{Goal} - p}{|p_{Goal} - p|} \tag{2}$$

$$U_{repulsive}^{(n)}(x) = \begin{cases} \frac{1}{2} K_{obs} \left(\frac{1}{d_{lidar}} - \frac{1}{d_{Max}} \right), & d_{lidar} < d_{max} \\ 000000000000000 \quad 0, & d_{lidar} \geq d_{max} \end{cases} \tag{3}$$

f_{Pull} : Potential Attraction

$U_{Repulsive}^{(n)}(x)$: Potential Rejection

k_{Pull} : Coefficient Potential pulls interesting

p_{Goal} : Position point destination (coordinates point destination)

p : Position final car

K_{obs} : Coefficient potential reject

d_{lidar} : Distance read by the Lidar sensor

d_{max} : Threshold value (safe threshold)

2.2.2. Vehicle Kinematic Model

To accurately describe the vehicle's movement, a kinematic model is established using a fixed reference point (I) and a reference point on the vehicle's frame, as depicted in Fig. 6. A Cartesian coordinate system is applied, where forward and backward movements occur along the Y-axis, while left and right movements occur along the X-axis. The vehicle's rotation angle is denoted as Ψ, while the velocity components along the Y and X axes are represented as U and V, respectively. Displacement along each axis is defined in (4) [45], where movements along the X-axis are assigned opposite directional values, with one component given a negative sign, whereas all Y-axis values remain positive [46]. The vehicle's movement direction, particularly when encountering obstacles, is determined using LiDAR sensor data and the vehicle's heading angle, as formulated in (5).

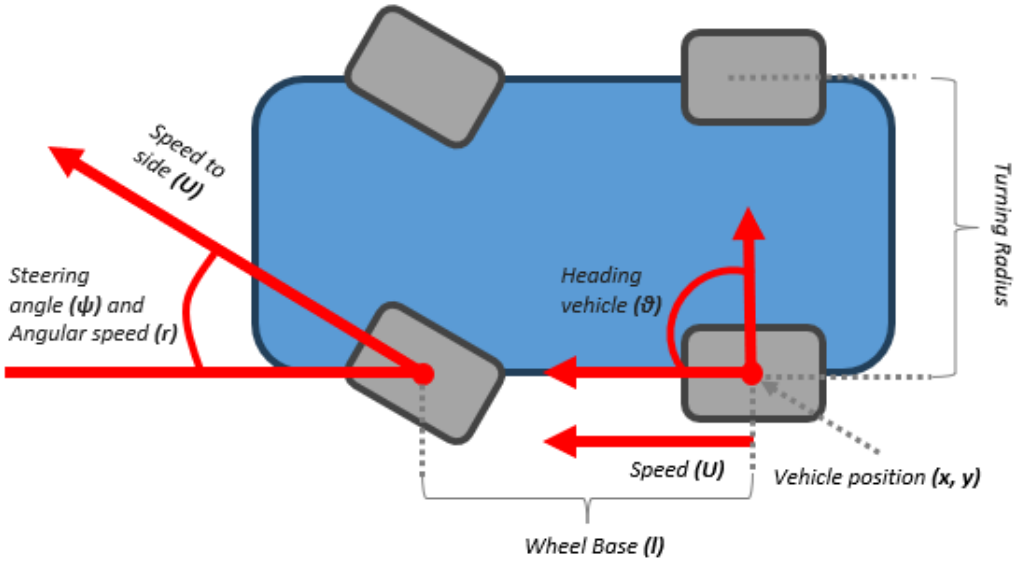

Fig. 6. Kinematic models of cars

$$\begin{bmatrix} X \\ Y \\ \Psi \end{bmatrix} = \begin{bmatrix} \cos\Psi & -\sin\Psi & 0 \\ \sin\Psi & \cos\Psi & 0 \\ 0 & 0 & 1 \end{bmatrix} \begin{bmatrix} U \\ V \\ r \end{bmatrix} \quad (4)$$

$$\begin{bmatrix} X \\ Y \\ \Psi \end{bmatrix} = \begin{bmatrix} U\cos\Psi - \mathrm{V}\sin\Psi \\ U\ \cos\Psi + \mathrm{V}\ \sin\Psi \\ r \end{bmatrix} \quad (5)$$

Description:

X = Displacement to the side (lateral)

Y = Displacement proceeds or back off

Ψ = *Angular* displacement

U = Speed moment forward and backward

V = Speed moment to side

r = Angular speed of the car

2.2.3. Dodger Crash System

The Dodger Crash System, illustrated in Fig. 7, integrates a GPS-based autonomous navigation system, which activates at the start of program execution. If the detected distance d_{Lidar} remains greater than or equal to the threshold d_{max}, the vehicle proceeds toward its target coordinates without interruption. However, if d_{Lidar} falls below d_{max}, the main program is interrupted by a collision avoidance subroutine [47], [48]. The first step of this subroutine involves calculating the X and Y coordinates using (6), based on distance and angle data received from the LiDAR sensor. These coordinates are used to compute the lengths of the X and Y axes, relative to the LiDAR readings, as determined in (7). Once these values are obtained, the system calculates the required displacement for the vehicle using (8), resulting in final displacement values (vx_{End}, vy_{End}) as specified in (9) [48]. To prevent excessive displacement, additional adjustments are made using (10). Once the recalculated displacement falls below d_{max}, the program resumes normal operation according to the conditions outlined in (9).

Through this approach, the system effectively enables real-time obstacle avoidance while maintaining an efficient navigation path. Further enhancements could include optimizing LiDAR data processing algorithms or integrating alternative path-planning techniques, such as A*[49], Dijkstra [50], or Rapidly-exploring Random Trees (RRT) [51], to improve decision-making in dynamic environments.

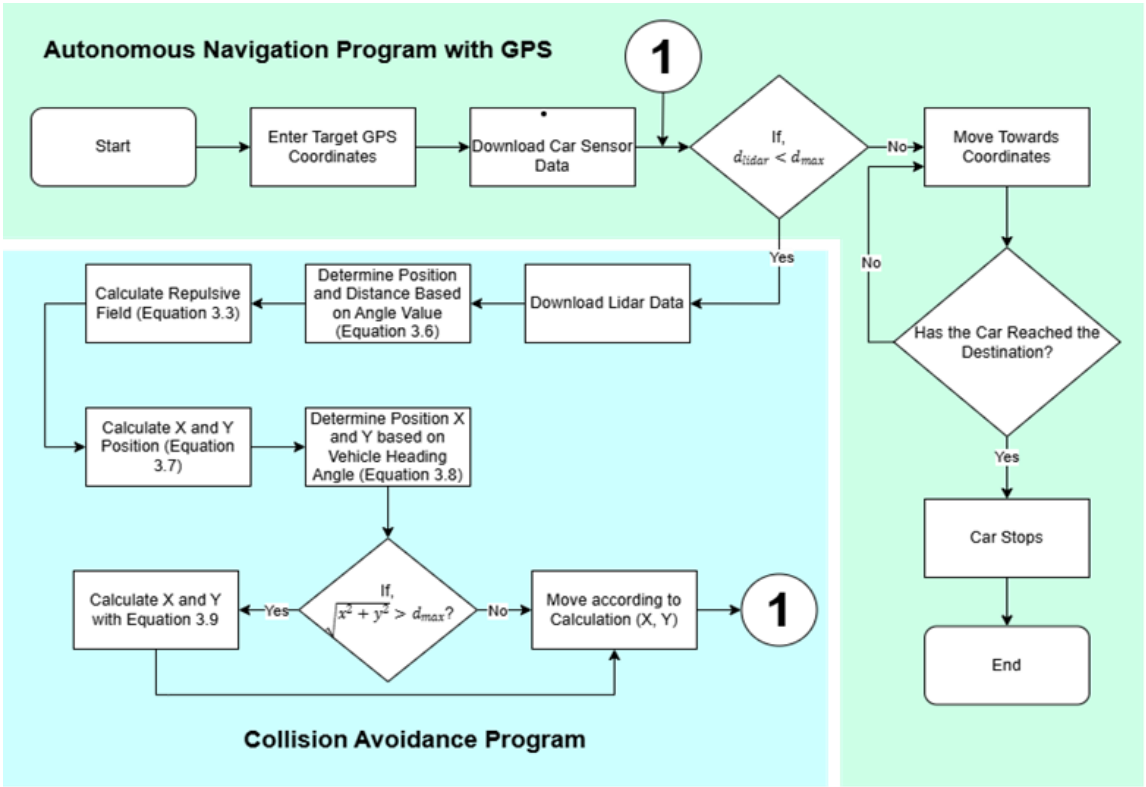

Fig. 7. Flowchart of the system dodger crash

$$\begin{cases} X_{lidar} = \cos\theta \times d_{lidar} \\ Y_{lidar} = \sin\theta \times d_{lidar} \end{cases} \quad (6)$$

$$\begin{cases} vx_{Lidar} = X_{lidar} \times U_{Repulsive}^{(n)}(x) \\ vy_{lidar} = Y_{lidar} \times U_{Repulsive}^{(n)}(x) \end{cases} \quad (7)$$

$$\begin{cases} vx_{End} = vx_{Lidar} \times \cos\theta - vy_{lidar} \sin\theta \\ vy_{End} = vx_{Lidar} \times \sin\theta + vy_{lidar} \times \cos\theta \end{cases} \quad (8)$$

$$Displacement = (vx_{End}, vy_{End}) \quad (9)$$

$$\begin{cases} vx_{End} = d_{max} \times \left(\dfrac{vx_{End}}{\sqrt{vx_{End}{}^2 + vy_{End}{}^2}} \right) \\ vy_{End} = d_{max} \times \left(\dfrac{vy_{Akhir}}{\sqrt{vx_{End}{}^2 + vy_{End}{}^2}} \right) \end{cases} \quad (10)$$

Where $+vxEnd, -vxEnd, +vyEnd, -vyEnd$ are stand for moving right, move left, move forward, and move backward, respectively.

3. Results and Discussion

3.1. Simulation Testing

The simulation was conducted by setting multiple GPS coordinate points as navigation targets for the car, with GPS accuracy playing a crucial role in ensuring precise navigation. The test utilized a trajectory with 12 waypoints, or reference GPS points, as illustrated in Fig. 8. The results indicate that the car successfully follows the predefined path, forming a trajectory that closely aligns with the programmed path. However, at higher speeds, the car exhibits a greater offset from the intended trajectory. This deviation is likely due to reduced response time and increased momentum, making rapid adjustments more challenging. Additionally, when waypoints are set either too close together or too far apart, some may not be detected due to each waypoint having an effective radius. Once the car enters this radius, the waypoint is considered passed, potentially leading to navigation inconsistencies in dense waypoint configurations.

The collision avoidance system is based on the potential field method and was simulated using Python's plotting tools to evaluate its effectiveness under different conditions. The simulation examined variations such as different threshold values and multiple obstacle scenarios. When navigating around two obstacles, the system's behavior remains similar to the single-obstacle case, except that the car performs two consecutive direction changes. Initially, it shifts to the left to avoid the first obstacle, like its response to a single obstacle, and then moves right to evade the second one. Once the second obstacle is cleared, the car returns to its original path, proceeding toward the target point, as illustrated in Fig. 9.

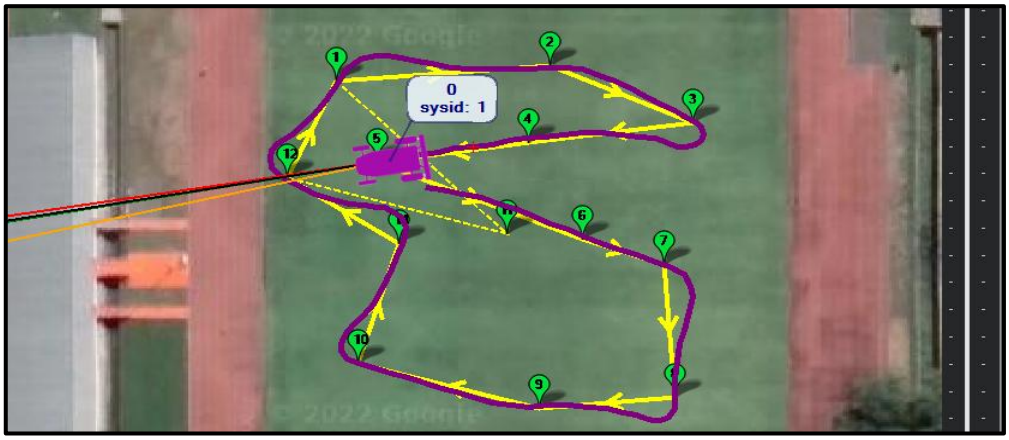

Fig. 8. Trajectory formed when carrying out missions

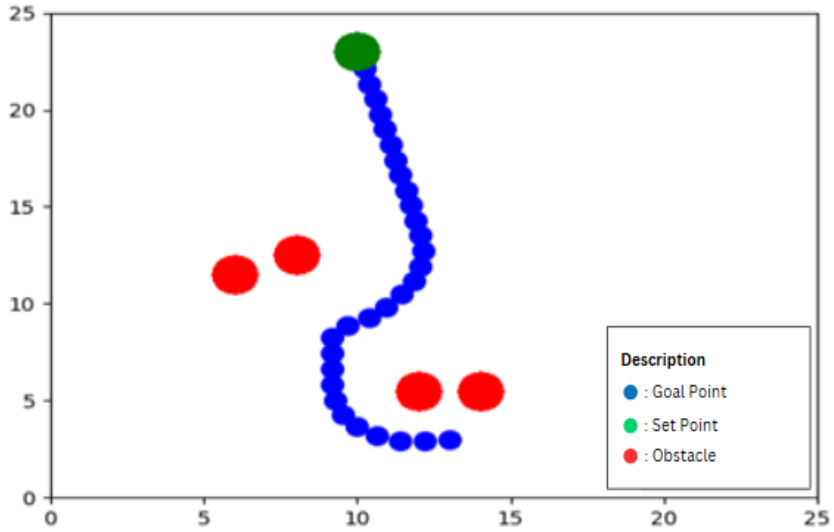

Fig. 9. Simulation results with 2 obstacles

3.2. Hardware Testing

Following successful simulation results demonstrating collision-free navigation, a prototype RC car was built and implemented, as shown in Fig. 10. The car was designed with a four-level structure to optimize space efficiency, with each level housing specific electronic components. In designing the collision avoidance system, the threshold or safety distance is a critical parameter. This threshold represents the minimum safe distance between the car and obstacles, determined using LiDAR sensor data. When an obstacle enters this range, the system activates, adjusting the car's trajectory to avoid collisions. If the object is outside the threshold, the system remains inactive. Selecting an optimal threshold is crucial: a small threshold may not provide sufficient time for the car to react, increasing the risk of collisions, while a large threshold may cause unnecessary deviations, slowing down the vehicle's progress.

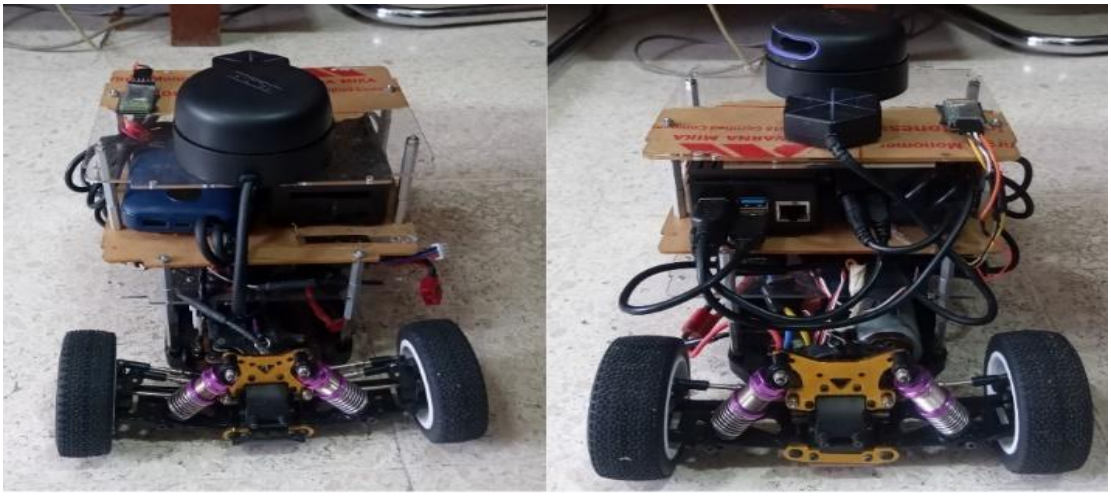

Fig. 10. Autonomous car prototype: (a) front view, (b) rear view

3.2.1. Sensor Testing

Accurate LiDAR sensor readings are essential for effective collision avoidance. Since LiDAR data primarily guides vehicle movement, a low margin of error is necessary for reliable navigation. To meet accuracy criteria, the error percentage should remain below 10%. Experimental results indicate that the accuracy achieved was approximately 96.40%, with an average error of 3.60%. Data collection involved 10 trials at 30 cm intervals, comparing LiDAR sensor measurements to manual

measurements using a meter stick. The calculations, based on (7), confirmed the sensor's high precision. Table 1 presents the measured data, showing that the sensor readings are sufficiently accurate to support the collision avoidance system.

The GPS module was tested through 50 trials to measure positioning accuracy. The test involved navigating a 14-meter distance between a starting point and a target point. The GPS coordinates, obtained from a Garmin GPS, were input into the vehicle's navigation system and executed 50 times. The actual stopping point of the vehicle was measured using a measuring tape to determine the error distance. The smallest error recorded was 22 cm (final trial). The largest error was 3 m (31st trial). The average error was 1.55 m, with a U-Blox-based GPS module offset of ~1.75 m.

The final stopping points of each test are depicted in Fig. 11. Out of 50 trials, the vehicle successfully reached the target circle in 33 trials, achieving an accuracy rate of 66%. The average number of satellites detected was 14, with an estimated travel distance of 15.5 m based on GPS data. Comparing actual distances with GPS readings, the average GPS error was approximately 0.59 m.

Table 1. Lidar testing results

No	Measured distance (cm)		Error (%)
	Tape measure	Lidar	
1	30	33	10
2	60	64	6.67
3	90	85	5.56
4	120	123	2.50
5	150	153	2.00
6	180	184	2,22
7	210	214	1.90
8	240	244	1,67
9	270	275	1.85
10	300	305	1.67
Mean of Error (%)		3.60	
Accuracy (%)		96.40	

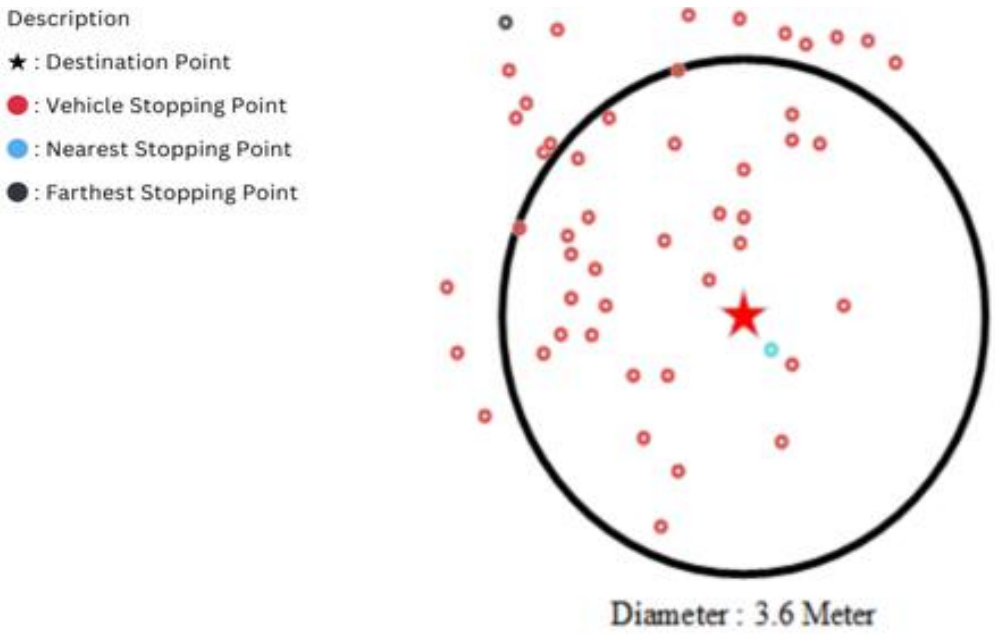

Fig. 11. GPS testing results

3.2.2. Collision Avoidance Testing

The study evaluated the collision avoidance system's effectiveness by testing two safety threshold values, 2 m and 2.5 m, with each threshold tested 10 times in scenarios involving one or

two obstacles along the vehicle's path. The experimental setup is shown in Fig. 12. When an obstacle entered the detection range, the system activated, adjusting the car's trajectory based on LiDAR data. In the single-obstacle test with a 2.5 m threshold, the error distance (distance to Point of Interest (POI)) ranged from 50 cm to 180 cm, with an average of 89.4 cm, as in Table 2. The shortest completion time recorded was 18.36 s with an error of 53 cm, while the longest was 19.98 s with an error of 180 cm, averaging 18.707 s. During these trials, an average of 16 satellites were detected, with an HDOP (Horizontal Dilution of Precision) of approximately 0.673, as shown in Fig. 13. In the two-obstacle test with the same threshold, error distances ranged from 78 cm to 185 cm, with an average of 135.6 cm, as resumed in Table 3. The shortest mission time was 18.2 s with an error of 100 cm, while the longest was 19.98 s with an error of 185 cm. The HDOP value averaged 0.679, with 16 satellites detected. These results suggest that the number of satellites and HDOP values significantly influence vehicle positioning accuracy, with higher satellite counts and lower HDOP values improving accuracy, while adverse weather conditions can reduce GPS precision.

Fig. 12. Obstacles of collision avoidance testing

Table 2. Test results 1 obstacle with a threshold of 2.5 m

Test	1 Obstacle			
	Distance to Point of Interest (cm)	Satellite Average	HDOP Average	Time (s)
1	180	14	0.691	19.210
2	50	18	0.641	18.680
3	98	15	0697	18.920
4	53	17	0.655	18.360
5	66	16	0.683	18.367
Average	89.4	16.6	0.673	18.707

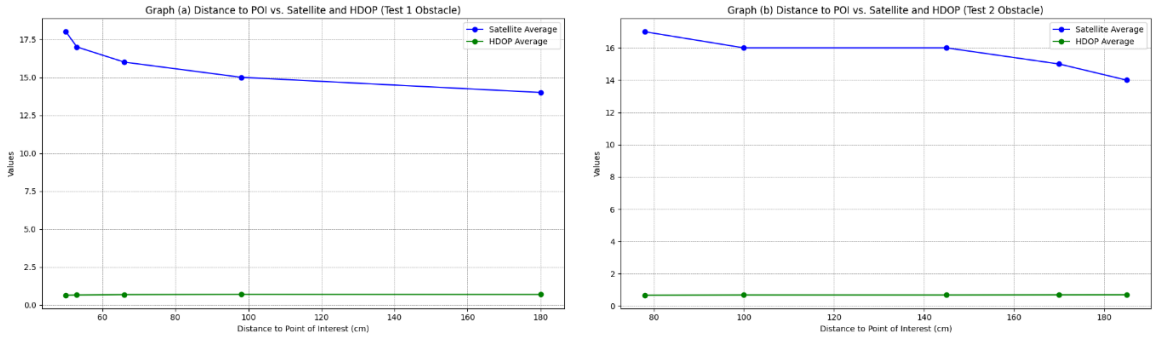

Fig. 13. (a) Graph distance to POI vs. Satellite and HDOP (Test 1 Obstacle), (b) Graph distance to POI vs. Satellite and HDOP (Test 2 Obstacle) at 2.5 Meter Threshold Value

Table 3. Test results for 2 obstacles with a threshold of 2.5 m

Test	2 Obstacles			
	Distance to Point of Interest (cm)	Satellite Average	HDOP Average	Time(s)
1	185	14	0.692	19.980
2	78	17	0.663	18.440
3	170	15	0.687	19.720
4	145	16	0.677	19.380
5	100	16	0.678	18.20
Average	135.6	15.8	0.679	19.144

To compare the impact of the two threshold values, key metrics such as travel distance, deviation from obstacle-free travel, and time differences were analyzed, with the results summarized in Table 4 and Fig. 14. With a 2 m threshold, the vehicle executed sharper turns, covering 16.406 m compared to 16.535 m with the 2.5 m threshold, while the baseline travel distance without obstacles was 15.5 m. The 2 m threshold resulted in an additional 0.432 m of travel distance, whereas the 2.5 m threshold added 0.447 m. The increase in travel time was 3.167 s for the 2 m threshold and 3.324 s for the 2.5 m threshold. Additionally, lower HDOP values improved GPS accuracy, helping the vehicle maintain a closer trajectory to the target.

Table 4. Test results with 1 obstacle

1 Obstacle		
Comparison	Threshold 2 m	Threshold 2.5 m
Average Mileage (m)	15.932	15.947
Average Time(s)	18.707	18.864
Margin to point destination (cm)	97.600	89.400

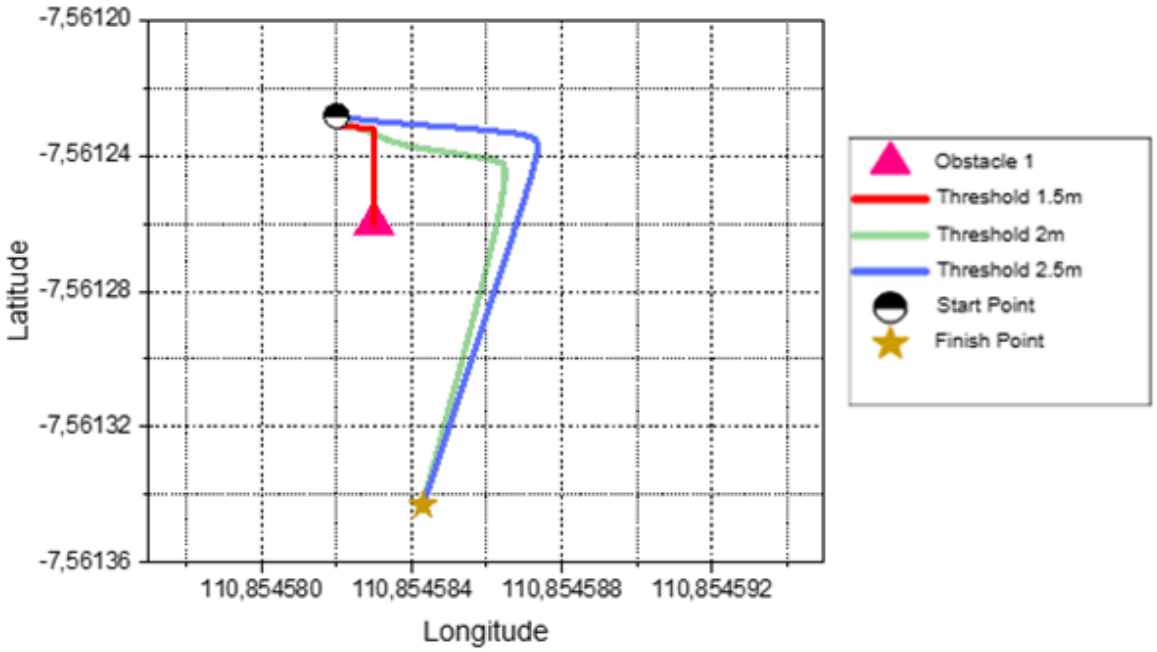

Fig. 14. Comparison trajectory when encountering 1 obstacle

For the two-obstacle navigation test, the track length and target point remained unchanged, but two obstacles were placed along the car's trajectory. The first obstacle, a pink object, caused the vehicle to veer left, as determined by a negative X-axis speed calculation. The second obstacle, an orange object, triggered a rightward adjustment since that path was closer to the target. Once both

obstacles were cleared, the collision avoidance system deactivated, allowing the vehicle to resume its GPS-based navigation. The results showed that with a 2 m threshold, the car traveled 16.406 m, while with a 2.5 m threshold, it covered 16.535 m. The additional travel distance with the 2.5 m threshold was 0.906 m. The average travel time was 19.036 s for the 2 m threshold and 19.144 s for the 2.5 m threshold. HDOP values fluctuated, with higher values reducing accuracy and lower values helping the car stay on the course. The results, summarized in Table 5 and Fig. 15, confirm that the collision avoidance system effectively navigates obstacles while maintaining reasonable accuracy. The choice of threshold impacts travel time, trajectory deviation, and the number of required directional changes.

Table 5. Test results with 2 obstacles

2 Obstacles		
Comparison	**Threshold 2 m**	**Threshold 2.5 m**
Average Mileage (m)	16.406	16.535
Average Time(s)	18.707	18.864
Margin to point destination (cm)	19.036	19.144

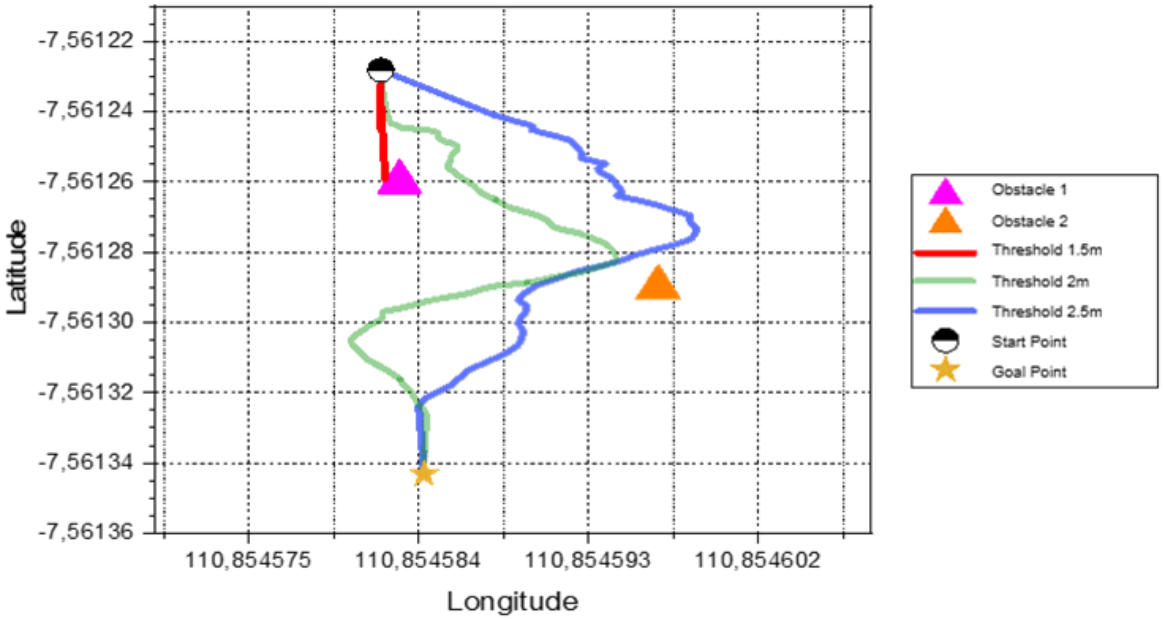

Fig. 15. Comparison trajectory moment facing 2 obstacles

4. Conclusion

The proposed collision avoidance system effectively navigates obstacles by integrating LiDAR-based detection and GPS positioning. Across multiple trials, the GPS-based autonomous mode achieved an average positioning error of 1.55 m, while LiDAR maintained an accuracy of 96.40%, exceeding the required 95% threshold. Testing with two safety thresholds (2 m and 2.5 m) demonstrated that both values enabled successful navigation, though the 2 m threshold resulted in a 0.8% shorter travel distance and a 0.6% faster completion time compared to the 2.5 m threshold. However, the 2.5 m threshold provided greater clearance, reducing close encounters with obstacles. The system's performance was also influenced by GPS accuracy, with lower HDOP values and higher satellite counts improving trajectory precision. Real-time trajectory adjustments ensured adaptive navigation in both single- and two-obstacle scenarios, confirming the system's reliability in dynamic environments. These findings highlight the importance of threshold selection in balancing efficiency and safety. Future work may explore adaptive threshold tuning based on real-time environmental conditions to further enhance system performance.

Author Contributions: Conceptualization, methodology, tools, software, validation, formal analysis, investigation, sources, power, data curation, compilation draft beginning writing, writing review and editing, and visualization have been done by all writers.

Acknowledgments: This research was supported by The Ministry of Education, Culture, Research, and Technology under the scheme of Applied Research – Downstream Pathway with contract number 1280.1/UN27.22/PT.01.03/2023.

Conflicts of Interests: The authors declare there is no conflict of interest.

References

[1] Y. Xing *et al*., "Driver Lane Change Intention Inference for Intelligent Vehicles: Framework, Survey, and Challenges," *IEEE Transactions on Vehicular Technology*, vol. 68, no. 5, pp. 4377-4390, 2019, https://doi.org/10.1109/TVT.2019.2903299.

[2] A. S. Mohammed, A. Amamou, F. K. Ayevide, S. Kelouwani, K. Agbossou, and N. Zioui, "The perception system of intelligent ground vehicles in all weather conditions: A systematic literature review," *Sensors*, vol. 20, no. 22, p. 6532, 2020, https://doi.org/10.3390/s20226532.

[3] A. Koesdwiady, R. Soua, F. Karray and M. S. Kamel, "Recent Trends in Driver Safety Monitoring Systems: State of the Art and Challenges," *IEEE Transactions on Vehicular Technology*, vol. 66, no. 6, pp. 4550-4563, 2017, https://doi.org/10.1109/TVT.2016.2631604.

[4] M. Q. Khan and S. Lee, "A Comprehensive Survey of Driving Monitoring and Assistance Systems," *Sensors*, vol. 19, no. 11, p. 2574, 2019, https://doi.org/10.3390/s19112574.

[5] S. K. Fondzenyuy, C. S. Fowo Fotso, S. L. T. Feudjio, D. S. Usami, L. Persia, "Self-Reported Speed Compliance and Drivers Speeding Behaviour in Cameroon," *Future Transportation*, vol. 4, no. 2, pp. 659-680, 2024, https://doi.org/10.3390/futuretransp4020031.

[6] N. Lubbe, H. Jeppsson, A. Ranjbar, J. Fredriksson, J. Bärgman, M. Östling, "Predicted road traffic fatalities in Germany," *IRCOBI conference 2018*, pp. 17-52, 2018, https://www.ircobi.org/wordpress/downloads/irc18/pdf-files/11.pdf.

[7] A. Zhirabok, A. Zuev, and K. C. Il, "Virtual Sensors Design for Nonlinear Dynamic Systems," *International Journal of Robotics and Control Systems*, vol. 3, no. 2, pp. 134–143, 2023, https://doi.org/10.31763/ijrcs.v3i2.915.

[8] W. Farag, "Traffic signs classification by deep learning for advanced driving assistance systems," *Intelligent Decision Technologies*, vol. 13, no. 3, pp. 305-314, 2019, https://doi.org/10.3233/IDT-180064.

[9] W. Farag and Z. Saleh, "Road Lane-Lines Detection in Real-Time for Advanced Driving Assistance Systems," *2018 International Conference on Innovation and Intelligence for Informatics, Computing, and Technologies (3ICT)*, pp. 1-8, 2018, https://doi.org/10.1109/3ICT.2018.8855797.

[10] O. Bouazizi, C. Azroumahli, A. El Mourabit, and M. Oussouaddi, "Road Object Detection using SSD-MobileNet Algorithm: Case Study for Real-Time ADAS Applications," *Journal of Robotics and Control (JRC)*, vol. 5, no. 2, pp. 551–560, 2024, https://doi.org/10.18196/jrc.v5i2.21145.

[11] J. S. Saputro *et al*., "Design of intelligent cruise control system using fuzzy-PID control on autonomous electric vehicles prototypes," *Journal of Mechatronics, Electrical Power, and Vehicular Technology*, vol. 15, no. 1, pp. 105–116, 2024, https://doi.org/10.55981/j.mev.2024.877.

[12] V. K. Kukkala, J. Tunnell, S. Pasricha and T. Bradley, "Advanced Driver-Assistance Systems: A Path Toward Autonomous Vehicles," *IEEE Consumer Electronics Magazine*, vol. 7, no. 5, pp. 18-25, 2018, https://doi.org/10.1109/MCE.2018.2828440.

[13] J. S. Saputro, A. H. D. Susilo, M. Anwar, Sutrisno and F. Adriyanto, "Design of Automatic Emergency Braking and Foward Collision Warning as a Collision Avoidance System Using Fuzzy Logic," *2024 7th International Seminar on Research of Information Technology and Intelligent Systems (ISRITI)*, pp. 516-521, 2024, https://doi.org/10.1109/ISRITI64779.2024.10963413.

[14] Z. Xu, X. Zhan, Y. Xiu, C. Suzuki and K. Shimada, "Onboard Dynamic-Object Detection and Tracking for Autonomous Robot Navigation With RGB-D Camera," *IEEE Robotics and Automation Letters*, vol. 9, no. 1, pp. 651-658, 2024, https://doi.org/10.1109/LRA.2023.3334683.

[15] H. -Y. Lin and X. -Z. Peng, "Autonomous Quadrotor Navigation With Vision Based Obstacle Avoidance and Path Planning," *IEEE Access*, vol. 9, pp. 102450-102459, 2021, https://doi.org/10.1109/ACCESS.2021.3097945.

[16] S. Y. Alaba and J. E. Ball, "Deep Learning-Based Image 3-D Object Detection for Autonomous Driving: Review," *IEEE Sensors Journal*, vol. 23, no. 4, pp. 3378-3394, 2023, https://doi.org/10.1109/JSEN.2023.3235830.

[17] W. Zhangyu, Y. Guizhen, W. Xinkai, L. Haoran and L. Da, "A Camera and LiDAR Data Fusion Method for Railway Object Detection," *IEEE Sensors Journal*, vol. 21, no. 12, pp. 13442-13454, 2021, https://doi.org/10.1109/JSEN.2021.3066714.

[18] Y. Song, Z. Xie, X. Wang and Y. Zou, "MS-YOLO: Object Detection Based on YOLOv5 Optimized Fusion Millimeter-Wave Radar and Machine Vision," *IEEE Sensors Journal*, vol. 22, no. 15, pp. 15435-15447, 2022, https://doi.org/10.1109/JSEN.2022.3167251.

[19] M. Hasenjäger and H. Wersing, "Personalization in advanced driver assistance systems and autonomous vehicles: A review," *2017 IEEE 20th International Conference on Intelligent Transportation Systems (ITSC)*, pp. 1-7, 2017, https://doi.org/10.1109/ITSC.2017.8317803.

[20] M. Hammer, M. Hebel, and M. Arens, "Automated object detection and tracking with a flash LiDAR system," *Proceedings Volume 9988, Electro-Optical Remote Sensing X*, 2016, https://doi.org/10.1117/12.2240640.

[21] M. Carfagni *et al*., "Metrological and critical characterization of the intel D415 stereo depth camera," *Sensors*, vol. 19, no. 3, p. 489, 2019, https://doi.org/10.3390/s19030489.

[22] M. T. Ohradzansky and J. S. Humbert, "Lidar-Based Navigation of Subterranean Environments Using Bio-Inspired Wide-Field Integration of Nearness," *Sensors*, vol. 22, no. 3, p. 849, 2022, https://doi.org/10.3390/s22030849.

[23] J.-S. Kim, D.-H. Lee, D.-W. Kim, H. Park, K.-J. Paik, and S. Kim, "A numerical and experimental study on the obstacle collision avoidance system using a 2D LiDAR sensor for an autonomous surface vehicle," *Ocean Engineering*, vol. 257, p. 111508, 2022, https://doi.org/10.1016/j.oceaneng.2022.111508.

[24] J. Park and N. Cho, "Collision avoidance of hexacopter UAV based on lidar data in dynamic environment," *Remote Sensing*, vol. 12, no. 6, p. 975, 2020, https://doi.org/10.3390/rs12060975.

[25] U. Z. A. Hamid *et al*., "Autonomous emergency braking system with potential field risk assessment for frontal collision mitigation," *2017 IEEE Conference on Systems, Process and Control (ICSPC)*, pp. 71-76, 2017, https://doi.org/10.1109/SPC.2017.8313024.

[26] M. Galvani, "History and future of driver assistance," *IEEE Instrumentation & Measurement Magazine*, vol. 22, no. 1, pp. 11-16, 2019, https://doi.org/10.1109/MIM.2019.8633345.

[27] D. Gruyer, V. Magnier, K. Hamdi, L. Claussmann, O. Orfila, and A. Rakotonirainy, "Perception, information processing and modeling: Critical stages for autonomous driving applications," *Annual Reviews in Control*, vol. 44, pp. 323–341, 2017, https://doi.org/10.1016/j.arcontrol.2017.09.012.

[28] A. Boubakri and S. M. Gamar, "A New Architecture of Autonomous Vehicles: Redundant Architecture to Improve Operational Safety," *International Journal of Robotics and Control Systems*, vol. 1, no. 3, pp. 355–368, 2021, https://doi.org/10.31763/ijrcs.v1i3.437.

[29] M. B. Alatise and G. P. Hancke, "A Review on Challenges of Autonomous Mobile Robot and Sensor Fusion Methods," *IEEE Access*, vol. 8, pp. 39830-39846, 2020, https://doi.org/10.1109/ACCESS.2020.2975643.

[30] F. Nashashibi and A. Bargeton, "Laser-based vehicles tracking and classification using occlusion reasoning and confidence estimation," *2008 IEEE Intelligent Vehicles Symposium*, pp. 847-852, 2008, https://doi.org/10.1109/IVS.2008.4621244.

[31] D. J. Natale, R. L. Tutwiler, M. S. Baran and J. R. Durkin, "Using full motion 3D Flash LIDAR video for target detection, segmentation, and tracking," *2010 IEEE Southwest Symposium on Image Analysis & Interpretation (SSIAI)*, pp. 21-24, 2010, https://doi.org/10.1109/SSIAI.2010.5483929.

[32] Y. Zeng *et al*., "An improved calibration method for a rotating 2D LIDAR system," *Sensors*, vol. 18, no. 2, p. 497, 2018, https://doi.org/10.3390/s18020497.

[33] N. S. Rao, E. Alekhya, M. N. Suleman, K. S. Nikhil, "Autonomous Obstacle Avoidance Vehicle using LIDAR and an Embedded System," *International Journal for Research in Applied Science & Engineering Technology*, vol. 8, no. 6, pp. 25–31, 2020, https://doi.org/10.22214/ijraset.2020.6005.

[34] J.-F. Duhé, S. Victor, and P. Melchior, "ContribUtions on Artificial Potential Field Method for Effective Obstacle Avoidance," *Fractional Calculus and Applied Analysis*, vol. 24, no. 2, pp. 421–446, 2021, https://doi.org/10.1515/fca-2021-0019.

[35] K. K. C. F. Nunes, T. T. Ribeiro and A. G. S. Conceicao, "Trajectory Planning with Obstacle Avoidance using APF and COLREGS for USVs," *2024 IEEE International Conference on Autonomous Robot Systems and Competitions (ICARSC)*, pp. 106-111, 2024, https://doi.org/10.1109/ICARSC61747.2024.10535946.

[36] D. Wang, H. Chen, S. Lao and S. Drew, "Efficient Path Planning and Dynamic Obstacle Avoidance in Edge for Safe Navigation of USV," *IEEE Internet of Things Journal*, vol. 11, no. 6, pp. 10084-10094, 2024, https://doi.org/10.1109/JIOT.2023.3325234.

[37] Fahmizal, D. Y. Kharisma, and S. Pramono, "Implementation of Fuzzy Logic Control on a Tower Copter," *Journal of Fuzzy Systems and Control*, vol. 1, no. 1, pp. 14–17, 2023, https://doi.org/10.59247/jfsc.v1i1.25.

[38] S. G. Nayak, A. Patil, and G. Gadagenavar, "Development and Analysis of Speed Control of BLDC Motor with Arduino Controller," *International Journal of Innovative Technology and Exploring Engineering*, vol. 11, no. 4, pp. 63-66, 2022, http://doi.org/10.35940/ijitee.C9813.0311422.

[39] B. A. Malyshev, P. A. Troshin, S. Y. Zanegin and D. M. Shishov, "Research of Electronic Speed Controllers Designs and Functional for Unmanned Aerial Vehicles," *2024 IEEE 25th International Conference of Young Professionals in Electron Devices and Materials (EDM)*, pp. 1150-1155, 2024, https://doi.org/10.1109/EDM61683.2024.10615216.

[40] N. J. H. Purnomo, A. A. Masroeri, W. H. Nugroho, and Sahlan, "Study on the Application of Microcontroller-Based GPS Sensors on Floater Gliders to Reach the Specified Destination," *IOP Conference Series: Earth and Environmental Science*, p. 12020, 2022, https://doi.org/10.1088/1755-1315/1081/1/012020.

[41] N. F. Muthmainnah, A. R. A. Tahtawi, and B. Baisrum, "Voltage Stability Control of Boost Converter Using Linear Quadratic Integrator," *Journal of Fuzzy Systems and Control*, vol. 1, no. 2, pp. 39–43, 2023, https://doi.org/10.59247/jfsc.v1i2.41.

[42] H. J. Jo, S. R. Kim, J. H. Kim, and J. Y. Park, "Comparison of Velocity Obstacle and Artificial Potential Field Methods for Collision Avoidance in Swarm Operation of Unmanned Surface Vehicles," *Journal of Marine Science and Engineering*, vol. 10, no. 12, p. 2036, 2022, https://doi.org/10.3390/jmse10122036.

[43] A. Lazarowska, "Comparison of Discrete Artificial Potential Field Algorithm and Wave-Front Algorithm for Autonomous Ship Trajectory Planning," *IEEE Access*, vol. 8, pp. 221013-221026, 2020, https://doi.org/10.1109/ACCESS.2020.3043539.

[44] Y. Koren and J. Borenstein, "Potential field methods and their inherent limitations for mobile robot navigation," *Proceedings. 1991 IEEE International Conference on Robotics and Automation*, vol. 2, pp. 1398-1404, 1991, https://doi.org/10.1109/ROBOT.1991.131810.

[45] J. S. Saputro, P. H. Rusmin and A. S. Rochman, "Design and Implementation of Trajectory Tracking Motion in Mobile Robot Skid Steering Using Model Predictive Control," *2018 IEEE 8th International Conference on System Engineering and Technology (ICSET)*, pp. 73-78, 2018, https://doi.org/10.1109/ICSEngT.2018.8606361.

[46] K. Yan and B. Ma, "Global Posture Stabilization for the Kinematic Model of a Rear-Axle Driven Car-Like Mobile Robot Considering Obstacle Avoidance," *IEEE Robotics and Automation Letters*, vol. 8, no. 9, pp. 5568-5575, 2023, https://doi.org/10.1109/LRA.2023.3296351.

[47] Y. Duan, C. Yang, J. Zhu, Y. Meng, and X. Liu, "Active obstacle avoidance method of autonomous vehicle based on improved artificial potential field," *International Journal of Advanced Robotic Systems*, vol. 19, no. 4, 2022, https://doi.org/10.1177/17298806221115984.

[48] J. H. Cho, D. S. Pae, M. T. Lim, and T. K. Kang, "A Real-Time Obstacle Avoidance Method for Autonomous Vehicles Using an Obstacle-Dependent Gaussian Potential Field," *Journal of Advance Transportation*, vol. 2018, no. 1, pp. 1-15, 2018, https://doi.org/10.1155/2018/5041401.

[49] Z. Lin, K. Wu, R. Shen, X. Yu and S. Huang, "An Efficient and Accurate A-Star Algorithm for Autonomous Vehicle Path Planning," *IEEE Transactions on Vehicular Technology*, vol. 73, no. 6, pp. 9003-9008, 2024, https://doi.org/10.1109/TVT.2023.3348140.

[50] S. Kim, H. Jin, M. Seo and D. Har, "Optimal Path Planning of Automated Guided Vehicle using Dijkstra Algorithm under Dynamic Conditions," *2019 7th International Conference on Robot Intelligence Technology and Applications (RiTA)*, pp. 231-236, 2019, https://doi.org/10.1109/RITAPP.2019.8932804.

[51] W. Ayalew, M. Menebo, C. Merga, and L. Negash, "Optimal path planning using bidirectional rapidly-exploring random tree star-dynamic window approach (BRRT*-DWA) with adaptive Monte Carlo localization (AMCL) for mobile robot," *Engineering Research Express*, vol. 6, no. 3, p. 35212, 2024, https://doi.org/10.1088/2631-8695/ad61bd.